Elsevier Editorial System(tm) for Materials and Design
Manuscript Draft

Manuscript Number:

Title: Effect of gate design and cavity thickness on filling, morphology and mechanical properties of microinjection moldings

Article Type: Original Article

Keywords: Micro gate design; size-induced crystallization; process-induced crystallization; long-term mechanical properties; morphology of micro scale features

Corresponding Author: Prof. Michael D. Gilchrist, PhD, DEng

Corresponding Author's Institution: University College Dublin

First Author: Nan Zhang, PhD

Order of Authors: Nan Zhang, PhD; Su Quanliang, MSc; Seong Ying Choi, PhD; Michael D. Gilchrist, PhD, DEng

Abstract: Miniaturized parts weighing single or tens of milligrams represent a large category of microinjection moulded products. Both miniaturization and extreme processing under microinjection moulding subject material to high shear rates and high cooling rates, and cause the same material to have different morphologies and final properties when used in conventional injection moulding. It also makes mold design challenging. This study investigates the effects of micro gate design (opening and thickness) and cavity thickness (100-500μm) on filling, morphology and the mechanical properties of miniaturized dumbbell parts. It is found that a reduction of gate size has two conflicting effects, namely, increased shear heating increases flow length, and increased cooling rate reduces flow length. Filling increases significantly with an increase of cavity thickness. In addition, the thickness of the skin layer reduces from ~70% to ~10% when part thickness increases from 100μm to 500μm. This oriented skin layer determines molecular orientation and broadly influences Young's modulus, elongation and yield stress. Natural aging at room temperature induces an increase of modulus and yield stress, and a decrease of strain at break. The mechanical properties of microinjection moldings is significantly different from those of conventional injection moldings and measurement at microscale is required for miniaturized product design.

Effect of Gate Design and Cavity Thickness on Filling, Morphology and Mechanical Properties of Microinjection Moldings

Nan Zhang, Quanliang Su, Seong Ying Choi, *Michael D. Gilchrist

School of Mechanical and Materials Engineering, University College Dublin, Ireland

*Corresponding Author: Michael Gilchrist

Email: michael.gilchrist@ucd.ie

Highlights

- Reducing gate size has conflicting effects on part filling
- Increasing cavity thickness can significantly increase polymer melt flow length
- Reducing part thickness increases skin ratio and molecular orientation which, in turn, significantly influence mechanical properties
- Natural aging increases modulus and yield stress, and decreases failure strain
- Design of microinjection molded products requires that special attention be given to material properties at the micro scale

Abstract

Miniaturized parts weighing single or tens of milligrams represent a large category of microinjection moulded products. Both miniaturization and extreme processing under microinjection moulding subject material to high shear rates and high cooling rates, and cause the same material to have different morphologies and final properties when used in conventional injection moulding. It also makes mold design challenging. This study investigates the effects of micro gate design (opening and thickness) and cavity thickness (100-500μm) on filling, morphology and the mechanical properties of miniaturized dumbbell parts. It is found that a reduction of gate size has two conflicting effects, namely, increased shear heating increases flow length, and increased cooling rate reduces flow length. Filling increases significantly with an increase of cavity thickness. In addition, the thickness of the skin layer reduces from ~70% to ~10% when part thickness increases from 100μm to 500μm. This oriented skin layer determines molecular orientation and broadly influences Young's modulus, elongation and yield stress. Natural aging at room temperature induces an increase of modulus and yield stress, and a decrease of strain at break. The mechanical properties of microinjection moldings is significantly different from those of conventional injection moldings and measurement at microscale is required for miniaturized product design.

Key words: Micro gate design; size-induced crystallization; process-induced crystallization; long-term mechanical properties; morphology of micro scale features

1. Introduction

In response to the trend for miniaturization of devices, products and components in the medical, optical and telecommunication industries, microinjection molding has been developed successfully as a mass production technology for small, high precision, high value-added products [1-3]. Microinjection molding involves two typical products: micro components weighing a few milligrams or large parts having micro/nano scale surface features. Such products have the common characteristic of a high surface to volume ratio, up to10^3~10^6 m^{-1}, and thus the cooling rate increases by the same order of magnitude [4]. Because of the intrinsic low thermal conductivity of polymer materials, a considerably high thermal gradient exists across the part thickness [1, 5, 6]. In order to fill such small features, high temperatures and high injection speeds are applied to reduce melt viscosity by shear thinning and these materials experience correspondingly high stresses and shear rates. Such a variable thermomechanical environment influences the nucleation and growth rate of crystalline entities and forms a special hierarchical microstructure for microinjection moldings.

Similar to conventional injection molding, micromoldings present typical "skin-core" structures, which are composed of highly oriented structures in the skin, a less-oriented transcrystalline layer and non-oriented spherulite crystals in the core. Depending on the type of materials, size and process conditions, morphological layers may be absent, especially when comparing a macro sample and a miniaturized sample. For example, when part thickness decreases to below 200μm, the spherulite core layer is absent and replaced by a shear layer with highly orientated shish-kebab structures for HDPE [5, 7], which is denoted as a "core-free" morphology. Formation of a shish-kebab structure in the core occurs because the shear rate is strong enough to convert point-like nuclei in the core region into fibril-like nuclei and the thermal gradient is high enough to limit relaxation of nuclei [8]. Thus, epitaxial growth of folded lamellae from fibril-like structures (shishes) leads to the formation of kebab structures. Except for such extreme conditions, the main morphology difference between micromoldings and conventional moldings is understood to be the relative thicknesses of different morphology layers, which determine the final physical properties of a component [5, 6, 9-13]. The orientated layers account for more than 90% of the entire thickness of a micro part (thickness < 0.2mm), which is 3~4 times higher than that of a macro part (thickness > 1.5mm) [5, 12, 13]. Additionally, HDPE micro parts have a much high level of molecular orientation along the flow direction from the

core to the skin compared to the macro part, while the corresponding crystallinity of a micro part is lower than a macro part, except for in the core region [7]. However, it was also reported that the overall crystallinity of HDPE [12] and PP [11] micro parts was higher than a macro part, which may because of differences between material grades and characterization methods. Some studies have also related part miniaturization to morphology and properties. Edmund & Marcel [14] compared the morphology and mechanical properties of four different miniaturized tensile bar specimens and found no uniform correlation between the geometry miniaturization to changes of the mechanical properties, although they claimed morphologies, like outer layer thickness, structure fineness and degree of crystallinity influenced mechanical properties, as known in conventional injection molding [15, 16]. Such an observation might also be due to different process conditions and tensile testing conditions. Jungmeier et al. [4] studied the influence of cooling rate on morphology and mechanical properties by scaling down a standard tensile specimen with a range of scale factors (1:2, 1:4, 1:8 to 1:16; corresponding part thickness 2, 1, 0.5 and 0.25mm), corresponding to different skin to volume ratios. Injection velocity was tuned to keep a consistent shear rate. It was found that crystal size, crystallinity and yield stress decreased with an increasing surface to volume ratio, because of the increasing cooling rate. The maximum fractions of skin layer were ~70% and ~30% for the studied materials, POM and PA66, respectively. For PA66, the Young's modulus and yield strength decreased by ~40% and ~10%, respectively, compared to manufacturer's data. For POM, on the other hand, modulus and yield strength did not have a monotonic variation with an increase of skin ratio, although the modulus was smaller and yield strength was similar to the manufacturer's data. Moreover, they found that the effect of the cooling rate due to the surface to volume ratio was more significant than the machine process parameters. Meister et al. [17], from the same group, carried out artificial aging to study the long-term mechanical properties of miniaturized tensile bars using PA66. Whether aged or not, the crystallinity of the skin reduced, while the core crystallinity increased, when the tensile bars were scaled down from 1:2 to 1:16. However, morphological observation did not identify any difference between before and after aging. Young's modulus decreased, yield strain increased, while strain at break presented no monotonic variation when scaling from 1:2 to 1:16. After aging, modulus and yield stress had increased while elongation had decreased and such effects became weaker when parts became smaller, which was related to post-crystallization and oxidation degradation. Interestingly, Lu and Zhang [18-20] analyzed the morphology and mechanical properties of PP micro arrays with diameters ranging from 60μm~130μm with height of 250μm, when produced by microinjection molding. All pillar arrays have a "skin-core" morphology with skin, shear zone and

spherulite core, which is similar to the base part. However, micro pillars have a relatively higher percentage of shear zone than the base part. The hardness of pillars seems to be independent of pillar size, while hardness and modulus of the same column increases from core to skin. However, this work did not investigate the influence of process, material and miniaturization on morphology and properties of micro scale features.

Besides product miniaturization induced crystallization, extreme processing (high temperature and fast injection) also alters morphology. Kamal et al. [6] studied process-morphology relationships for 300μm POM parts and found that the skin layer decreased and the core layer increased with an increase of injection velocity and mold temperature. Thickness of skin, fine spherulites and twisted lamellae layers gradually decreased from the gate to the part end, due to the combined effects of melt velocity, pressure and temperature. The skin layer accounted for ~16%-26% of part thickness. Our recent work [21] systematically studied the effect of process on morphology evolution and mechanical properties of Poly(ether-block amide) (Pebax 7233) based on a 400μm thick miniaturized tensile specimen. It was found that both the thickness of the highly oriented skin layer decreased with an increase of injection velocity and mold temperature, while transcrystalline layers, such as fine-grained and oblate layers, increased with mold temperature; this trend was similar to what occurs in conventional injection molding [22]. A special spherulite-free core was found when a high cooling rate was applied. Some irregular "large spherulite" structures were seen to form beneath the skin layer because of the temperature increase caused by local shear heating. The skin layers occupied ~10%~32% of the cross-section, depending on processing conditions. Such a skin layer was composed of highly oriented structures and determined the degree of molecular orientation. We successfully demonstrated that a threshold level of shear stress existed to control the formation of a highly oriented skin layer. The coupled effects of shear rate and cooling rate determined the final morphology and eventual mechanical properties, especially for micromoldings.

The gate in injection molding is designed to ensure that polymer flows at a fast speed and with good liquidity in the filing stage; it needs to remain open long enough for additional material to be injected into the cavity to compensate for shrinkage [23]. The gate is also the thinnest section of molded articles, which serves to isolate the mold cavity from the sprue and runner, and it should solidify before the molded article does in order to prevent molten polymer from flowing back into the runner. Regarding microinjection molding, a flow analysis involving a typical 500μm gate is very different from modeling flow though a sub-100μm gate, because of inaccuracy regarding viscosity, heat transfer coefficient, etc. A micro part with micro gates would manifest more heating from the

polymer passing though such a small orifice, while it would experience high cooling rates because of the high surface to volume ratio. Thus, gate design would influence part filling behavior and would also impart material properties, especially for such heat-sensitive materials as bioresorbable and biopharmaceutical polymers, and thus it plays an important role in micro mold design. In recent years, a number of studies have been carried out on gate design. However, detailed design of a micro gate is still rare. In conventional injection molding, Pantani et al. [24] found that both gate thickness and cavity thickness affected the freeze-off time and they related gate solidification time to cavity pressure-time curves. Their analytical model was used successfully to estimate gate solidification time. Tor et al. [25] studied the influence of the ratio of width to depth of rectangular gates on the filling and the density of powder injection molded parts. They found that gates with larger depths might lead to higher weights and densities. Xie and Ziegmann [26] investigated the effect of gate dimensions on micro injection molded weld line strength. Their gates ranged from $0.025mm^3$ to $0.075mm^3$ and they found that a gate with larger width and smaller thickness would give the strongest weld line strength for micromoldings. However, the coupling of gate dimensions and processing conditions makes this effect rather complex. Recently, Xie et al. [23] used a visualizing mold to study the filling behavior of a conventional dumbbell part with different size gates ranging from $2mm^3$ to $24mm^3$. Jetting and short shot were found when using a small gate, which were coupled with processing conditions. Residual stress was significantly influenced by gate size, and larger gates led to parts with lower stresses.

Although much work has examined the evolution of microinjection moldings, very few have related morphology development to mechanical properties; those that have, fail to present clear results or present contradictory results. Both process and size induced crystallization are significant at the small scale; however, almost none of these compares the effects of extreme processing and miniaturization. In addition, almost none considers the morphology of micro surface features. As mentioned above, the gate is a crucial aspect of micro mold design and modeling flow behavior though a micro gate is particularly challenging. Therefore, experimental gate design and its influence on filling and morphology can give more insight into flow behavior though a micro gate and can assist in gate optimization. Following our previous study on process, morphology and mechanical properties for Pebax 7233 micro parts [21], the present work endeavors to study the morphology distribution in a micro part with special attention being given to 100 μm and sub-100μm features. The effect of the openings and thickness of micro gate on filling behavior is revealed by measuring part flow length and by evaluating the morphology distribution of the part. The effect of cavity thickness on morphology and mechanical properties is examined at the micrometer

scale, where part thicknesses decrease from 500µm to 100µm. The long-term mechanical properties of such small parts under natural conditions has also been investigated and related to morphology.

2. Experimental methods

2.1 Mold design

A series of dumbbell shaped mold inserts were used to form cavities with depths of 100µm, 200µm, 300µm, 400µm and 500µm, as shown in Figure 1. The volume of the micro part is less than three standard polymer pellets (Figure 1 (c)), with detailed dimensions as shown in Figure 1 (d). Interchangeable gate inserts form the gate using either convergent or divergent openings, as demonstrated in Figures 1 and 2. Detailed dimensions of the gate insert are listed in Table 1, where gate thickness and opening angle are the design variables. Gates A, B and C have divergent angles of 35º with gate width fixed at ~1.57mm and the thickness varying from 0.21mm to 0.08mm. Gates D and E open divergently (60º) and their width is fixed at ~2.46mm. Gates A and E have a similar thickness, as do gates B and D, based on measurements using scanning electron microscopy. Additionally, a 100µm slot was machined on both ends of the dumbbell of the stainless steel inserts using wire-electrical discharge machining. The corresponding features are shown in Figure 3, along with 40µm and 20µm wide features.

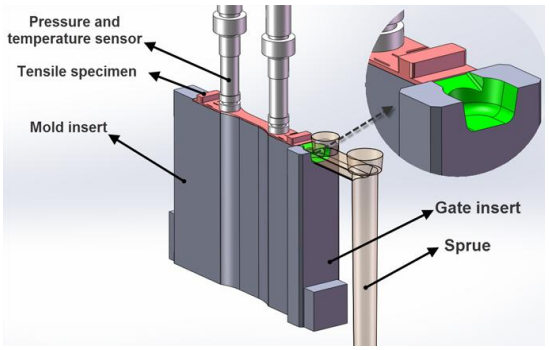

(a)

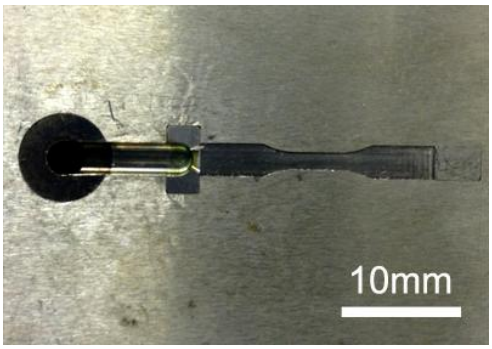

(b)

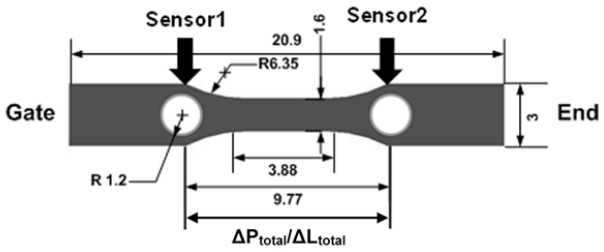

(c) (d)

Figure 1. Mold inserts and micromolded part: (a) assembly of cavity insert, gate inserts, sensors and parts; (b) corresponding assembly in the real mold, (c) micro part and (d) its planar dimension.

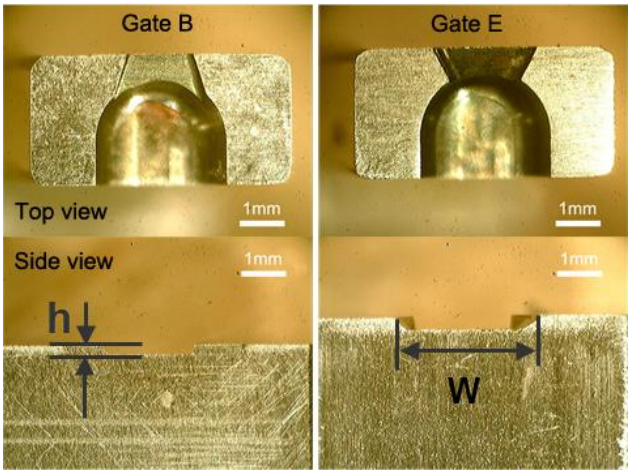

Figure 2. Gate inserts with convergent (gate B) and divergent (gate E) openings and various thicknesses (h: thickness, w: width)

Table 1. Dimensions of gate inserts (all dimensions in mm).

Gate	**Convergent (35º)**			**Divergent (60º)**	
	A	**B**	**C**	**D**	**E**
Width	1.54	1.56	1.6	2.43	2.49
Thickness	0.21	0.16	0.08	0.17	0.21

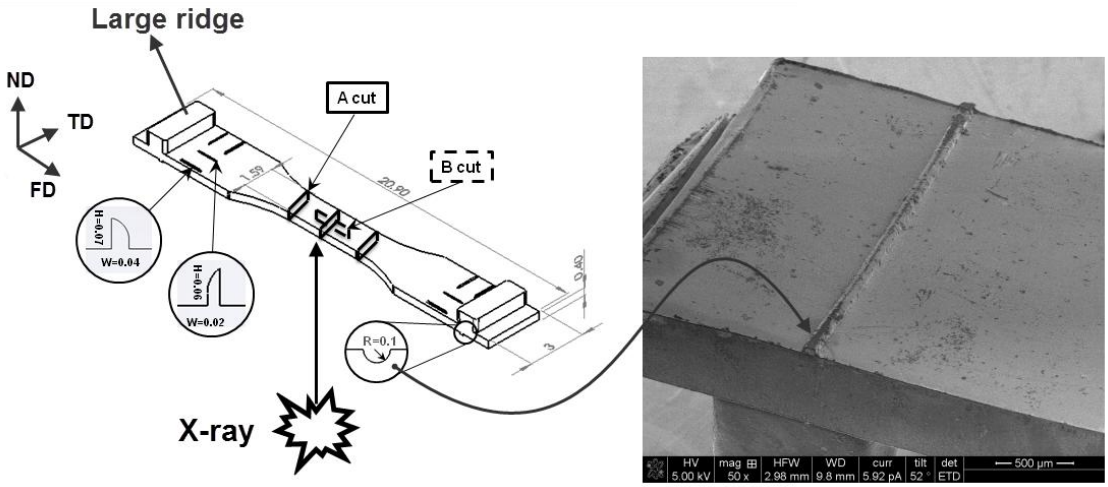

Figure 3. Sample sectioning (units: mm): A cut is along ND-TD plane, B cut is along ND-FD plane. Two 100µm features (SEM image) are located at the clamping end of the dumbbell samples, and 40µm and 20µm ridge features are aligned either along the flow direction or against the flow direction near the large clamping ridge. FD, ND and TD denote the polymer melt flow direction, normal direction and transverse direction, respectively.

2.2 Materials and processing conditions

Pebax 7233 SA01 (Melt Mass Flow Rate 5.5g/10min) was purchased from Arkema in pellet form and was used in the present study. It consists of 80% hard segments of polyamide-12 (PA12) and 20% soft segments of poly (tetra-methylene oxide) (PTMO) by molecular weight [27]. Microinjection molding experiments were carried out using a Fanuc Roboshot S-2000i 15B reciprocating microinjection molding machine, equipped with an injection screw with a diameter of 14mm. Relevant processing conditions are listed in Table 2. In cases where the gate effects were being studying, the mold temperature was increased to 110^{o}C in order to achieve more filling. Additionally, the samples were stored in a HDPE sample bag under room temperature conditions for more than a year to test for natural aging. The long-term mechanical properties were analyzed regarding various thicknesses under a miniaturized dumbbell part.

Table 2. Processing conditions for injection molding various specimens.

Nozzle temperature	Injection velocity	Holding pressure	Holding time	Mold temperature	Cooling time

210ºC	250mm/s	70MPa	1s	100º C	15s

Note: the mold temperature is increased to 110ºC in the study into gate effect in order to obtain more filling.

2.3 Characterization

The crystalline morphology was characterized using polarized light microscopy (PLM). Thin sections (10μm) were made along the ND-TD and TD-FD planes using a Leica EM UC 6 ultra-thin microtome, as shown in Figure 3. Small/Wide angle X-ray Scattering (SWAXS) was carried out using an Anton Paar SAXSess instrument, operated at 40kV and 50mA with point collimation (beam size ~0.3×0.2mm^2) and finger-like beam stop. The distance between sample and detector was 261.2mm. A CuKa radiation has been used with wavelength 0.154nm (PAN analytical X-ray source). Scattering from oriented samples was radially averaged and was converted into a 1D profile in order to determine the degree of orientation. The background under high vacuum conditions (0.1milli-Pa) was subtracted from the scattered intensity when calculating the orientation factor. All the samples were exposed under X-ray for 1 hour in transmission mode though the thickness direction. The orientation of crystalline lamellae was quantified in the form of the Herman's orientation function from the 2D-SAXS scattering patterns, according to Equations 1 and 2 [28]:

$$f = \frac{3\left\langle \cos^2 j \right\rangle - 1}{2} \tag{1}$$

$$\left\langle \cos^2 j \right\rangle = \frac{\int_0^{p/2} I(j)\cos^2 j \, dj}{\int_0^{p/2} I(j)\, dj} \tag{2}$$

where φ is the angle between the reference direction and the normal direction of a lamella. In the present case, the reference direction is defined to be the flow direction. If all the polymer chains are aligned parallel to the reference direction, $f = 1$. For an isotropic system, $f = 0$. If the polymer chains lie in a plane perpendicular to the reference direction, f has a value of -1/2.

Thermal analysis was carried out using a Mettler Toledo DSC 823e/500/670. The temperature profile consists of a heating stage followed by a cooling stage between 25ºC and 220ºC, at a rate of 10ºC/min. The crystallinity of a copolymer is calculated as:

$$\%Crystallinity = \left\{ x \times \frac{(\Delta H_{m,PA12} - \Delta H_{c,PA12})}{\Delta H_{PA12,100}} \times 100\% \right\} + \left\{ y \times \frac{(\Delta H_{m,PTMO} - \Delta H_{c,PTMO})}{\Delta H_{PTMO,100}} \times 100\% \right\} \quad (3)$$

where x is the weight fraction of polyamide, $\Delta H_{m,\,PA12}$ is the heat required to melt the crystals in the PA12 phase, $\Delta H_{c,PA12}$ is the enthalpy of the cold-crystallization in the polyamide phase, and $\Delta H_{PA12,\,100}$ is the theoretical heat of fusion for 100% crystalline PA12; y is the weight fraction of PTMO, $\Delta H_{m,\,PTMO}$ is the heat required to melt the crystals in the PTMO phase, $\Delta H_{c,\,PTMO}$ is the enthalpy of the cold-crystallization in the PTMO phase, and $\Delta H_{PTMO,\,100}$ is the theoretical heat of fusion for 100% crystalline PTMO. The weight fraction of polyamide was 0.8, determined elsewhere [33], which is based on the ratio of PTMO and PA 12. ΔH_m is a normalized enthalpy value calculated from the area of the melting peak, while $\Delta H_{100,PA12}$ is assumed to be 246 J/g [33]. Since no PTMO melting peak is observed around 7°C, the second term of Equation (3) is negligible.

2.4 Numerical simulation

In order to understand morphology development and gate effects, numerical simulation is used to qualitatively describe the flow and transfer during filling process. Autodesk Moldflow Insight (AMI) was used to simulate the polymer filling process of the dumbbell part **(**see Figure 1 (c)**).** Since there is no Pebax 7233 data in the AMI database, we used Pebax 7033 data instead, which has 75% PA12 and 25% PTMO by molecular weight, similar to 7233 [27]. The profile of screw speed vs. time during filling stage, and packing pressure vs. time during the packing stage of the injection-molding machine from the corresponding experiments were monitored using in-line process monitoring, as described in our previous work [10], and they are manually input into AMI to reflect real molding characteristics that are as realistic and precise as possible. The component together with the sprue were meshed using triangle elements and these elements were then converted into three dimensional tetrahedral elements for

simulation. Sequences of 10 tetrahedral elements were generated in the thickness direction. In total, the number of meshed tetrahedral elements was more than 3.6 million. All the results used in this work correspond to the time at the end of part filling.

2.5 Mechanical properties

Uniaxial tensile testing was carried out to obtain bulk mechanical properties of micro dumbbell specimens. The large ridges of the samples were fitted into clamping slots on a specially designed holder so as to eliminate any slippage. The specimens were positioned axially in the middle of the clamp and screwed down. The pre-tightening force was then released before being tested under tension. The tensile speed was set as 5mm/s, in accordance with ASTM D638-03 for semi-rigid plastics. To get statistically reliable data, 5 tensile tests were carried out for each condition. Material mechanical properties were characterized by Young's modulus, tensile yield stress and nominal strain at break. Young's modulus was approximated by the secant modulus at 5% strain.

3. Results and discussion

3.1 Morphology distribution

Pebax micro dumbbell parts show the typical "skin-core" morphology, regardless of whether they are cut along the transverse or flow direction, as shown by polarized light microscopy in Figure 4. Such morphology is made up of four distinct layers: skin, fine-grained, oblate and core layers. Details on the evolution of such morphology layers can be found in our previous work [21].

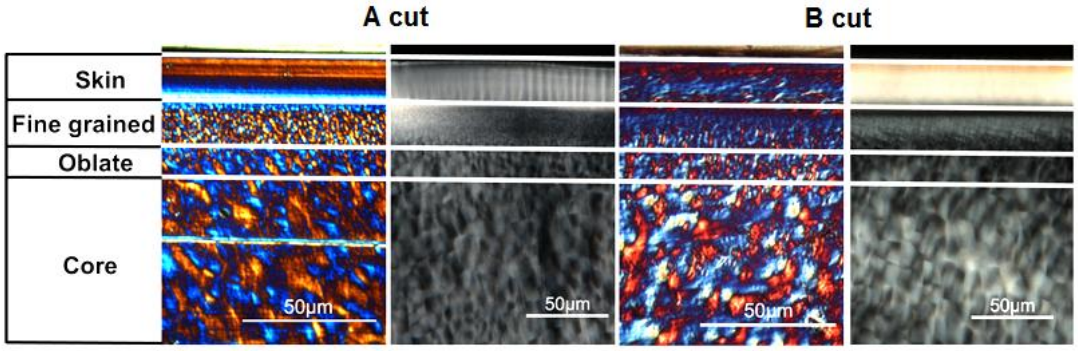

Figure 4. Morphology distribution at the same cross-section (c.f. Figure 3)

The distribution of morphology along the flow direction is influenced by the flow regime and heat transfer, both of which are closely related to the thermomechanical history that polymer melt experiences during its journey

to its final position in a molded part. Figure 5 exhibits the morphology distribution of a 400μm thick dumbbell part, cut along the flow direction (ND-FD plane, c.f. Figure 3) into seven zones. Emphasis is given to variations of morphological features within the 1st, 4th and 7th zones.

Figure 5. Morphology distributions along ND-FD plane of a 400μm thick part.

As shown in Figure 6, the 1st zone displays the morphology of the gate, large ridge region and a 100μm semi-circle feature (c.f. Figure 3). Because of the residual stress, thin sections made by microtoming are curled and the area seems smaller than examined on the remaining part. The gate region (1st zone (around region B in Figure 6)) exhibits some irregular patterns without any visible spherulitic structures. They are mixed with some spherulites. These irregular patterns are also observed at the very beginning of the part's edge. The reduced cross-sectional area of the gate causes pressure to increase, the main consequences of which are melt acceleration and flow elongation, as indicated by the shear rate distribution in Figure 6 (c). When hot melt is forced to flow into a cold cavity, a solidified layer forms promptly when the melt first contacts the cold mold wall. High shear and elongation stresses promote the number of point nuclei, which is evidenced by the fine spherulitic crystals in this shear-influenced region. Shear heating can introduce additional heat and re-melt the solidified layer formed at the gate region, leading to the mixture of spherulites and irregular non-spherulite patterns, as reported by Chu et al. on POM [29]. Additionally, when polymer melts flow from a small gate into a large cavity, the compressed melt springs back to form a radial flow field distribution, as evidenced by the distribution of morphology (Figure 6 (b)) and shear rate (Figure 6 (c)). A visible structure transition from small spherulites to large spherulites is observed (1st zone (around region A in Figure 6)). Since the shear rate decreases when melt flows into the cavity (Figure 6 (c)), shear induced nucleation gradually reduces the flowing pattern of the shear rate. At the same time, the combined effect of viscous heating, heat convection and heat conduction influences local thermal gradients and causes a radial distribution and a transition from a non-crystallizing zone to a zone of small and large spherulite crystals. When the part is fully filled, the temperature distribution around the gate looks even, except for additional heat being created by shear heating at the edges, which corresponds to the irregular amorphous patterns. A similar observation can be seen at the beginning of the part, with a transition of microstructure from the part center to its edge that follows the temperature

distribution, as inferred by the size reduction from center to edge. However, flow plays a more important role to determine the morphology around the gate region, as indicated by the radial distribution of morphology.

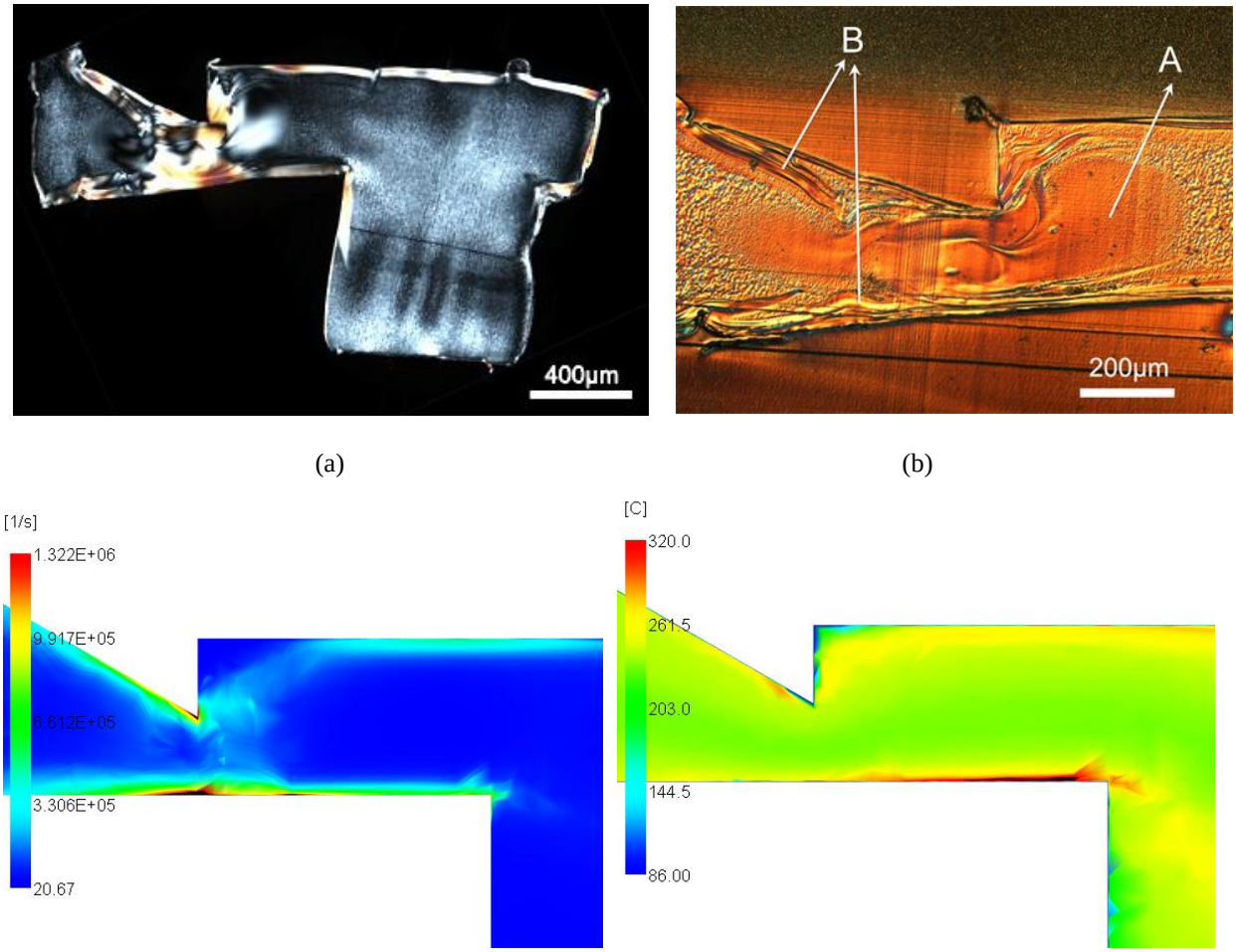

Figure 6. Morphology of 1st zone using transmission polarized light and reflection-polarized light: (a) morphology by transmission PLM and (b) reflected PLM, and the simulated maximum shear rate (c) and temperature (d) distribution around gate.

The 4th zone represents morphologies in the middle of the part, as shown in Figure 7 (a). The microstructures, especially the skin layer and oblate layer, are not identical at the upper and bottom surfaces of the part. This is because the mold temperatures of the moving half and the stationary half are not exactly the same and it leads to a thermal gradient through the thickness direction. The thickness of the morphological layers does not change significantly along the flow direction over a 2mm distance. As shown in Figure 7 (c), the shear rate has a relatively uniform distribution along the flow direction for 2mm and it transitions from a high shear region around the part

edge to a lower shear region in the core. We can observe a temperature transition from the part edge to the center (Figure 7 (d)), which corresponds very well to the skin (fast solidification and shear layer), fine-grained and core layers. A high shear rate can create fibril-like nuclei, which will grow into oriented structures at the skin layer, as suggested by molecular orientations measured by SAXS in Section 3.3.2.

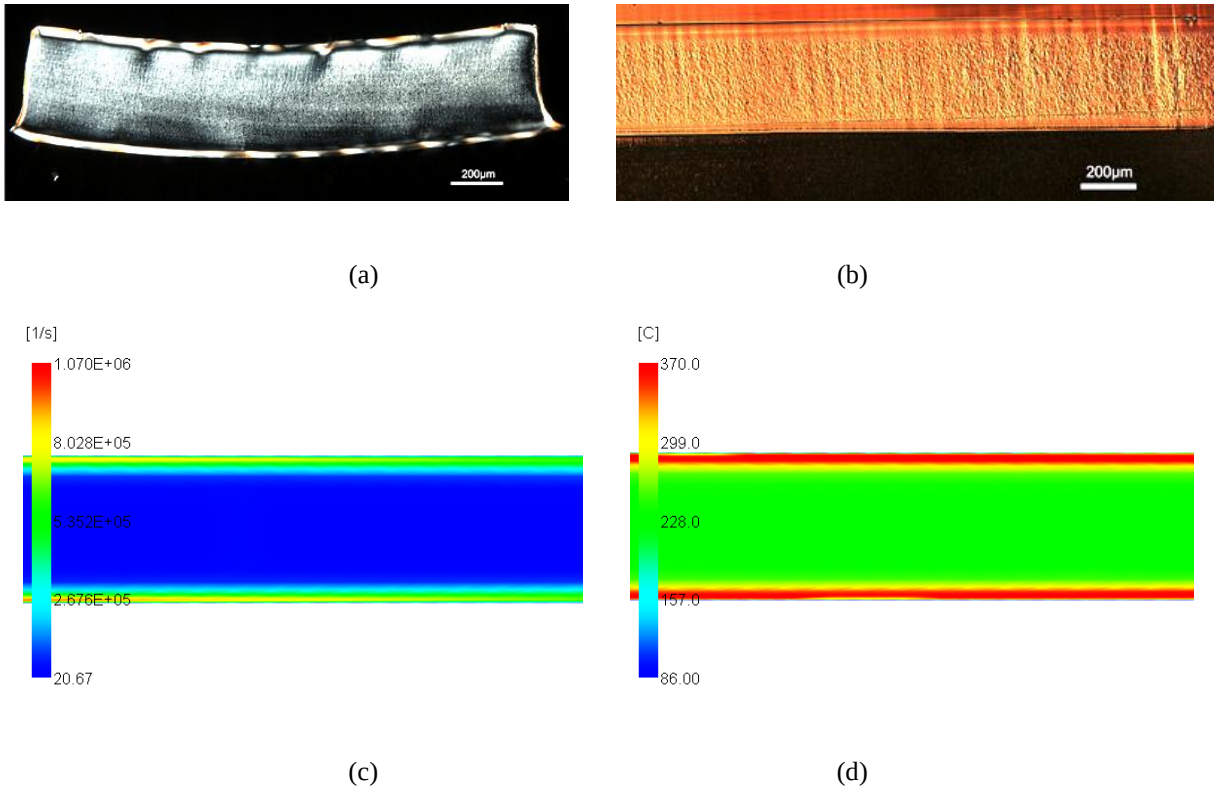

Figure 7. Morphology of 4th zone using transmission polarized light (a) and reflection polarized light (b), and predicted maximum shear rate (c) and temperature distribution when the part is fully filled (d).

The 7th zone shows the morphology near the large ridge and a 100µm micro feature, as displayed in Figure 8. In contrast to the central sections, such as the 4th zone, the skin layer disappears when the melt front passes by the large ridge (c.f. Figure 3). This is because at the end of the part, the shear is much smaller (Figure 8 (c)) and may not be sufficient to create fibrillar nuclei and, instead, point nuclei will form at random sites. Random nucleation finally leads to spherulitic crystals occupying most of the space towards the part's end with an ultra-thin skin and transcrystallization layers following the thermal gradient. Such analysis is supported by simulation (Figure 8 (c) and (d)) where the temperature increase by shear heating disappears when the melt front passes by the large ridge and the temperature appears uniform at the end of the part, which facilitates the growth of spherulite crystals.

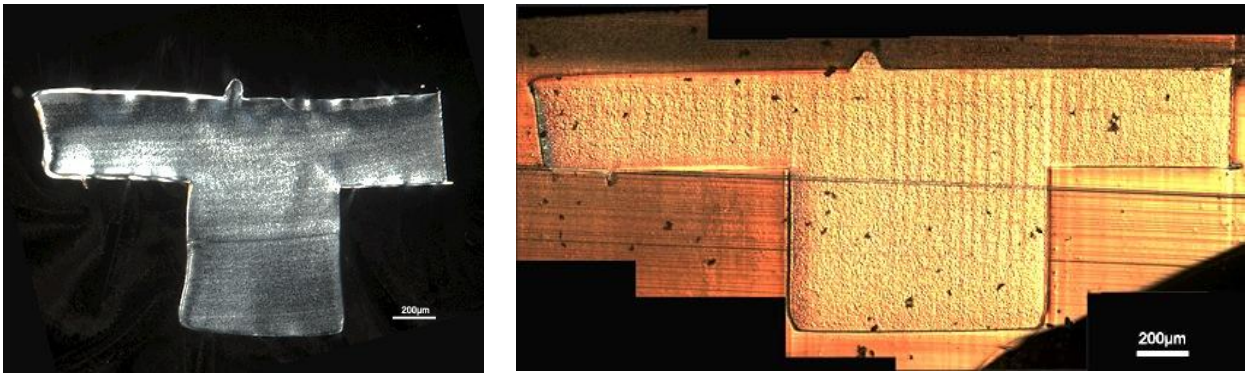

(a) (b)

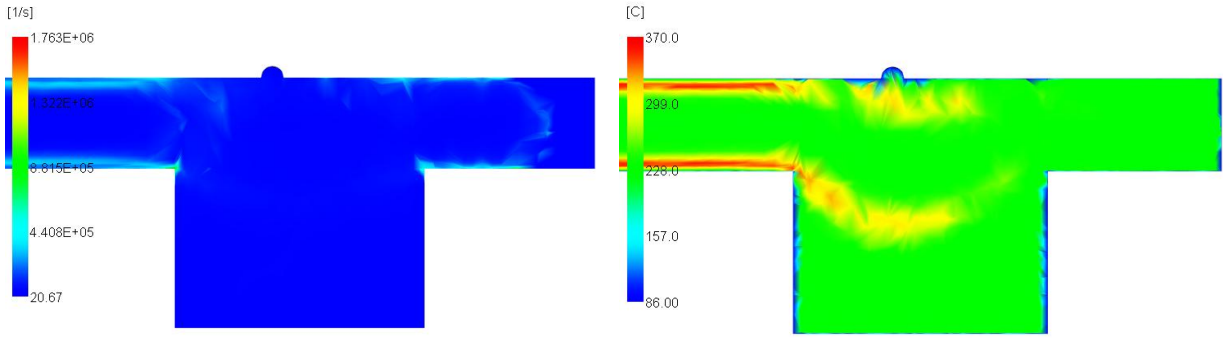

(c) (d)

Figure 8. Morphology of 7th zone using transmission polarized light (a) and reflection polarized light (a), and the predicted maximum shear rate (c) and temperature distribution when the part is fully filled (d).

The variation of morphology layers along the length direction is indicated in Figure 9. The thickness of the skin layer generally decreases from the gate to the part end. The fine-grained and oblate layers increase in thickness along the flow direction from ~2.5mm to ~15mm away from the gate. The thickness of the core layer is almost constant until ~15mm away from the gate, after which it increases. This distribution is similar to what has previously been observed for conventional injection molding [30, 31]. In microinjection molding, wall slip happens due to high shear stresses. This could reduce the molecular orientation slightly. At the same time, because of the high surface to volume ratio, the high thermal gradient causes a thicker skin layer in microinjection molding than in conventional injection molding. The decreasing skin layer thickness along the flow direction is due to the effect of hear transfer and a reduction of melt velocity along the flow direction. A reduction of velocity along the flow direction leads to smaller stresses. Fibril-like nucleation will not happen towards the interior of the part and the

thickness of the shear layer will finally reduce. Heat loss during filling can create a thicker solidified layer. The thickness of the fine-grained layer and oblate layer increases at a distance from 2.5mm to 15mm away from the gate. The reduced thickness of the skin layer along the flow direction leads to more significant heat transfer. Increased heat loss crystallizes more polymer melt along the thickness direction, creating thicker fine-grained and oblate layers. The thickness of the core layer does not change until 15mm away from the gate, where polymer melt reaches the large ridge that exists at the part's end. This ridge provides a large space for the fast moving melt and leads to a significant reduction of flow velocity and shear stress, which reduces point and fibril nucleation with decreasing thickness of the skin and fine grained layers. More space will consequently allow for random larger spherulites to be created.

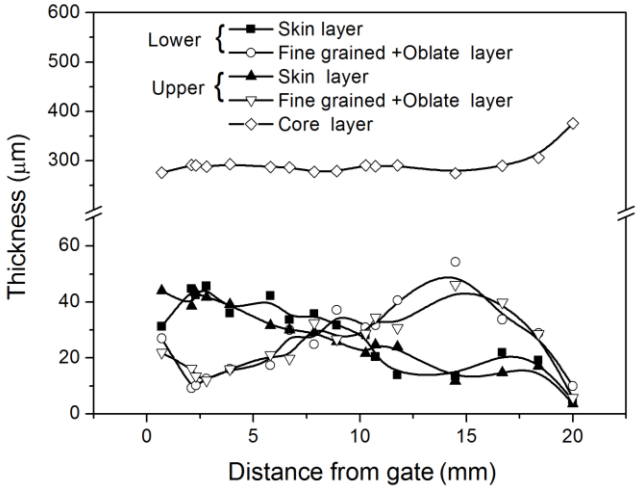

Figure 9. Variation of thickness of different morphological layers.

3.2 Morphology of micro features

Figure 10 shows the morphology of the 100μm features molded with Pebax and HDPE. The features near the gate and the part end present very different morphologies. Both of the HDPE features near the gate and part end have a similar microstructure to that of the skin layer beneath them, which indicates that the shear rates filling the features are large enough to create the oriented structures. The flow pattern is curved severely around the feature that is near the gate. A possible explanation for this is that the feature does not fully fill the micro cavity and the skin layer is then forced into the micro cavity by the pressure of subsequent melt. The feature that is far away from the gate does not display such severe curvature because of the low melt pressure at the end of the part.

For Pebax, the feature near the gate has a similar bent skin layer, which presents as a bright birefringence pattern similar to the skin layer. The feature is fully occupied by large spherulites except for a very thin, transparent, and fast solidification layer, as shown in Figure 10 (e). This implies that the shear rates filling this feature are too low to form highly oriented structures, compared to HDPE (Figure 10 (f)). However, the significant bending of the shear layer beneath the feature implies that the melt pressure near the gate is sufficiently high to cause large bending deformation. No such bent layer is present for the corresponding feature at the part end for Pebax, as shown in Figure 10 (d). This feature has a large spherulite structure with a fast solidification layer existing on the external surface. The bent skin layer is also present in the feature near the gate under conditions that lead to a non-spherulitic core, as shown in Figure 10 (f). In this case, the features have the same structure as the core with a thin transparent rapidly formed solidification layer on the external surface. Such effects of melt pressure on feature replication and part mechanical properties have not yet been studied. Similar to the two sub-100μm features (c.f. Figure 3), the 40μm features (c.f. Figure 11 (b)) consist of mainly large spherulite crystals. However, the 20μm features (c.f. Figure 11 (a)) appear to contain no visible spherulite crystals, which is because of the very high cooling rate. Of course, the microstructure of features depends on the material. One must be careful when designing a product with micro/nano features, since they possess various morphologies, which are different from in the macro part.

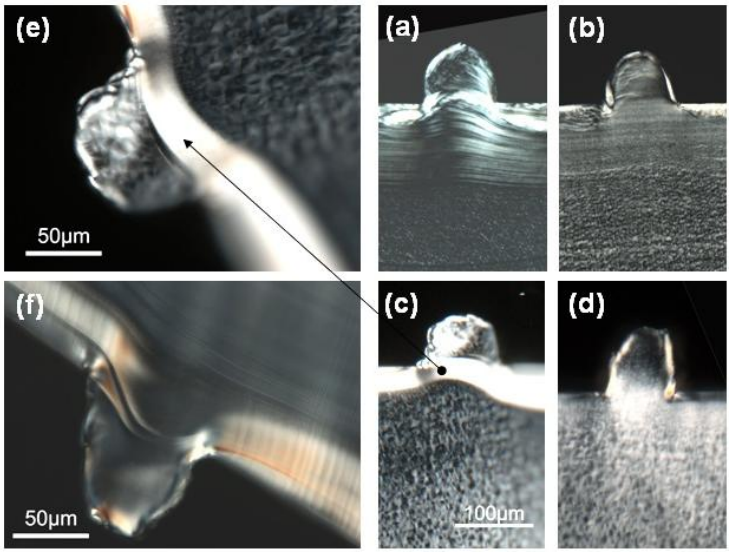

Figure 10. Morphology of 100μm features (c.f. Figure 3): (a) near gate (HDPE), (b) far away from gate (HDPE), (c) near gate (Pebax), (d) far away from gate (Pebax), (e) enlarged feature (c), (f) for cases without large spherulitic core (Pebax).

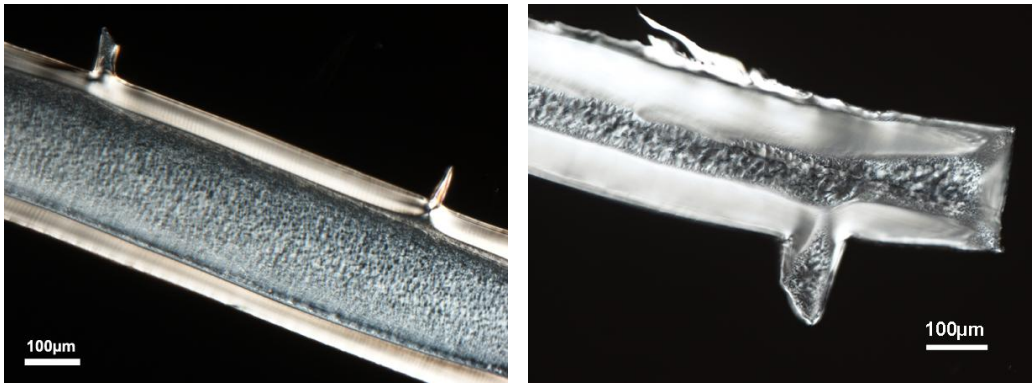

(a) (b)

Figure 11. Morphology of sub-100 micro features with a) 300µm and b) 100µm substrate.

3.3 Effect of mold design on filling and morphology

3.3.1 Effect of gate design

Figures 12 (a) and (b), and Table 2, show the influence of gate size on the flow length of a dumbbell part, where the cavity thickness is 100µm and 200µm, respectively. For the 100µm thick cavity, the maximum flow length is achieved by gate A, which has the largest thickness. Gates B and C give a similar flow length, regardless of gate thickness. When changing to the 200µm cavity, the best filling is achieved by gate D. The divergent and convergent openings exhibit conflicting effects on filling. For example, gate A gives more filling than gate E, but, gate B provides less filling than gate D. Cavity thickness significantly affects flow length, as indicated in Figure 12 (c), where only gate D is used. When cavity thickness increases from 100µm to 200µm, flow length increases from 5.12mm to 16.47mm. It is fully filled when cavity thickness exceeds 300µm. Obviously, cavity thickness has a more significant effect on filling. Additionally, when comparing the effect of gates A Vs B and gates D Vs E, there is no monotonic variation, which indicates that the gate openings have a less significant effect on the flow length.

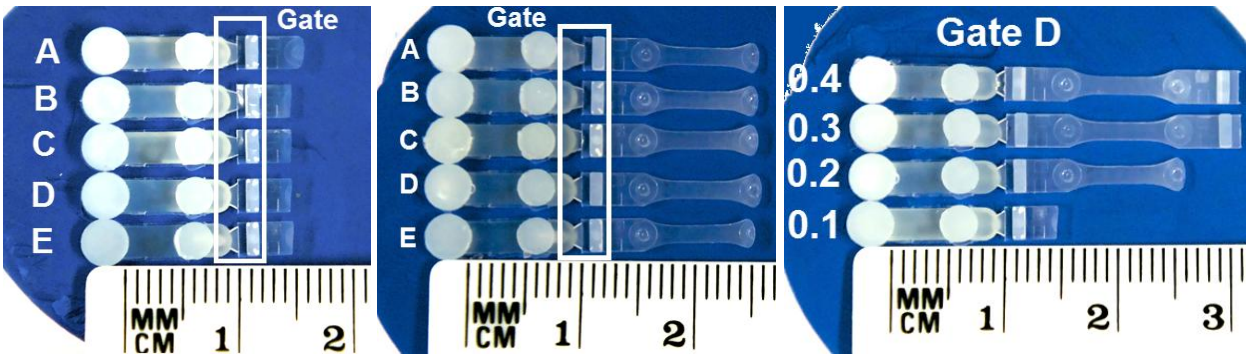

(a) (b) (c)

Figure 12. Comparison of flow length of dumbbell cavity with gates A-E when cavity thickness is 100μm (a), 200μm (b) and cavity thicknesses from 100μm and 400μm with gate D (c).

Table 2. Dumbbell part flow length (unit: mm)

Thickness \ Gate	A	B	C	D	E
100μm	5.47±0.35	5.01±0.03	5.06±0.23	5.19±0.17	5.20±0.16
200μm	16.15±0.15	16.07±0.12	15.91±0.51	16.47±0.16	15.69±0.29

Flow length is directly related to gate solidification, provided that the gate is the thinnest section of the part. In other words, once the gate solidifies, no more material can be supplied by the injection molding nozzle through the runner and sprue, and filling stops immediately, resulting in a short shot. Gate solidification only takes place when the heat lost though the gate walls by conduction overcomes the energy entering the gate from the runner because of convection. As described by Pantani et al [24], the conductive heat lost by transverse conduction in the gate, here denoted as Q_{cond}, is of the order of

$$Q_{cond} = \frac{4 \cdot d \cdot h}{b} \cdot k_s \cdot (T_s - T_w) \tag{3}$$

where k is thermal conductivity (the subscript "s" refers to the solid state), d, h and b are the gate width, length and thickness, respectively; T_S and T_w are the solidification and wall temperature, respectively. The amount of heat, Q_{conv}, that the material must dissipate in order to reach its solidification temperature, T_S, can be written as,

$$Q_{conv} = L \times W \times S \times c_{pm} \times (T_o - T_s) \times \frac{dr}{dt} \tag{4}$$

where L, W and S are cavity length, width and thickness, respectively, c_{pm} is the specific heat of polymer melts, and T_0 is the injection temperature, ρ is melt density and t is time. Q_{cond}, as calculated by Eq. (4), is time independent and is determined only by cavity geometry and molding conditions. On the other hand, Q_{conv} is proportional to the mass flow rate crossing the gate, which is a function of time. If the process, material and cavity thickness are fixed, heat loss by conduction is controlled by gate geometry. However, viscous heating as a heat source is not considered in this analysis. Reducing gate thickness has two conflicting effects, namely (i) increasing the heat lost by conduction and shortening the gate solidification time, and (ii) increasing the amount of shear heating and the gate solidification

time. These conflicting effects mean that the gate has a complex and non-monotonic influence on the filling behavior. For micro gates thinner than 100μm, even when the shear rate is as high as 10^6 s^{-1}, shear heating is still not sufficient to compete with heat conduction, as implied by a reduction of flow length in Table 2. For example, the corresponding flow length of the thinnest gate C with the same cavity thickness is smaller, as evidenced in Table 2. When using a fixed gate, filling increases from 5.19 to 16.47mm when cavity thickness changes from 100 to 200μm; it is fully filled for the 300 and 400μm cavities, as shown in Figure 12 (c). This implies that cavity thickness has a more significant effect on solidification time than the gate itself, especially at the micro scale. Compared to a conventional gate, a micro gate has a high surface to volume ratio and experiences more shear heating and solidifies faster. Numerical simulation of the polymer melt flow through such features can be a powerful tool for gate design and optimization. However, accurate simulation of micro features requires that more work should be done on melt rheology and heat transfer at the micro scale; such work is beyond the scope of this present paper.

Figure 13 compares the morphology at the gate and the region near the melt front. Numerical simulation of the filling behavior of gates A and C with a cavity thickness of 200μm is used to explain the morphology formation, as shown in Figure 14. It is obvious that gates A, B, D and E are thicker than the 100μm cavity, and that the gate is not the first part to solidify. For these gates, structures at the gate region are mainly spherulite crystals, except for the fast solidified layer around the edge. Such a spherulite crystallization region gradually reduces at the beginning of the part, as characterized by a large fraction of shear-influenced layers. Such morphology distribution is also seen for gates A and E, when cavity thickness increases to 200μm, where the gate size is larger than the part thickness. However, when the gate size becomes smaller than the cavity thickness, for example, gate C with cavity thickness 100μm and gates B, C and D with cavity thickness 200μm, the polymer melt accelerates at the gate region and expands when it flows into the cavity, similar to the flow behavior around the gate, as stated previously in Section 3.1. Some turbulent flow and possible back flow vortex are also observed for gate C at the beginning of the part, suggesting the possible occurrence of jetting. Almost no spherulite crystals were observed in the high shear region from the gate to the large clamping ridge when gate size is reduced to ~80μm (gate C at 200μm cavity). As shown in Figure 14 (a) and (b), the shear rate around the edge is one order of magnitude higher than in the center region, when gate thickness reduces from 200μm to 70μm (gate A to C). Gate A, with a 200μm cavity, has a uniformly distributed shear rate, while gate C, with a 200μm, cavity only accelerates at the gate region. Obviously, the smaller gate leads to an increase of the local temperature, as can be seen by comparing Figures 14 (c) and (d). But such additional

shear heating is still not enough to keep the gate open to permit more filling, when gate thickness is smaller than 100μm. The morphology near the flow front presents with a uniform morphology distribution from the skin to the spherulite core, indicating a steady shear and thermal gradient around the part edge in the shear zone. From this point, gate design itself influences much of the morphology of the gate region, except for the flow front. This might also be because the part is not fully filled and no possible back flow occurs. Actually, a micro gate should be sized to be smaller than the cavity thickness in order to prevent possible back flow and re-heating of the polymer melts, similar to in a conventional mold design. However, a possible larger ratio of gate to thickness would help filling. One must be careful, however, when gate thickness is smaller than 100μm.

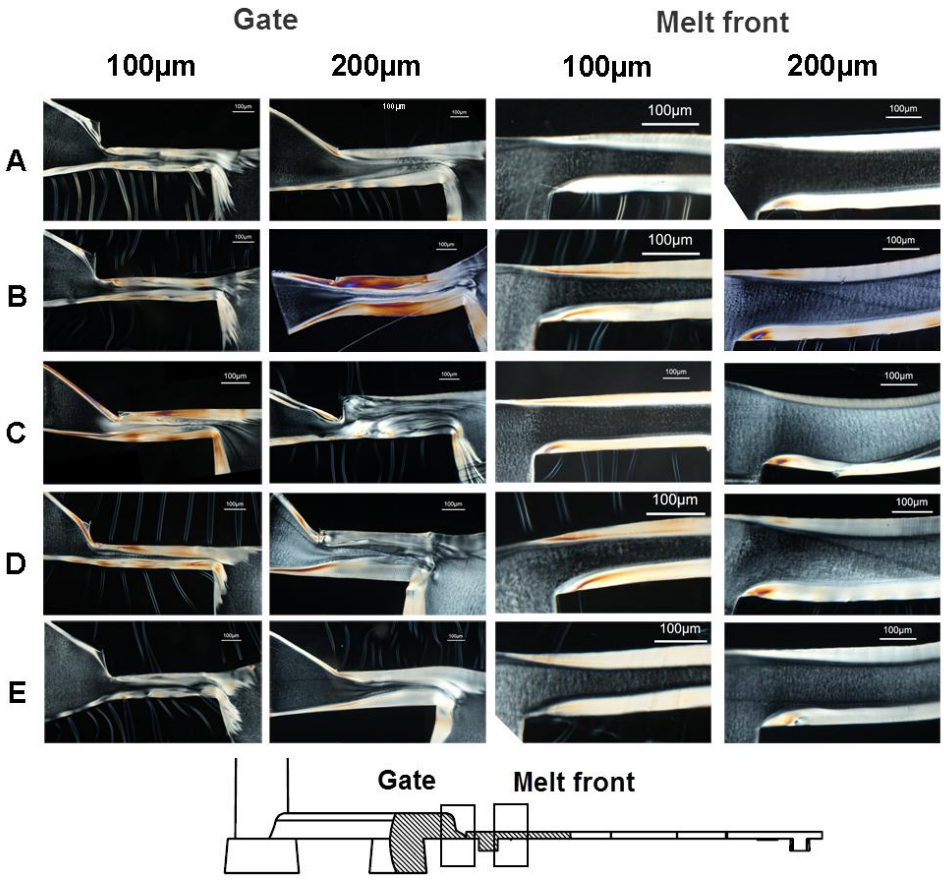

Figure 13. Morphology distribution at (a) gate and (b) region near melt front. A-E corresponds to the five different gate geometries (c.f. Table 1) for 100μm and 200μm cavity thicknesses.

3.3.2 Effect of cavity thickness

The morphology of micro parts with a thickness varying from 100μm to 500μm is shown in Figure 15, where the 100μm thick part was not fully filled and only the region near the gate was imaged. It is seen that the oriented skin occupies 67% and 50% of the 100μm and 200μm thick parts, respectively, which is much higher than parts thicker than 300μm (Figure 16). The skin ratio reduces significantly when cavity thickness exceeds 200μm, because of the increased cooling rate and shear rate. Jetting occurs when filling the 100μm part, leading to a non-uniform morphology distribution. However, it is difficult to determine the size variation of spherulites from solely PLM observations.

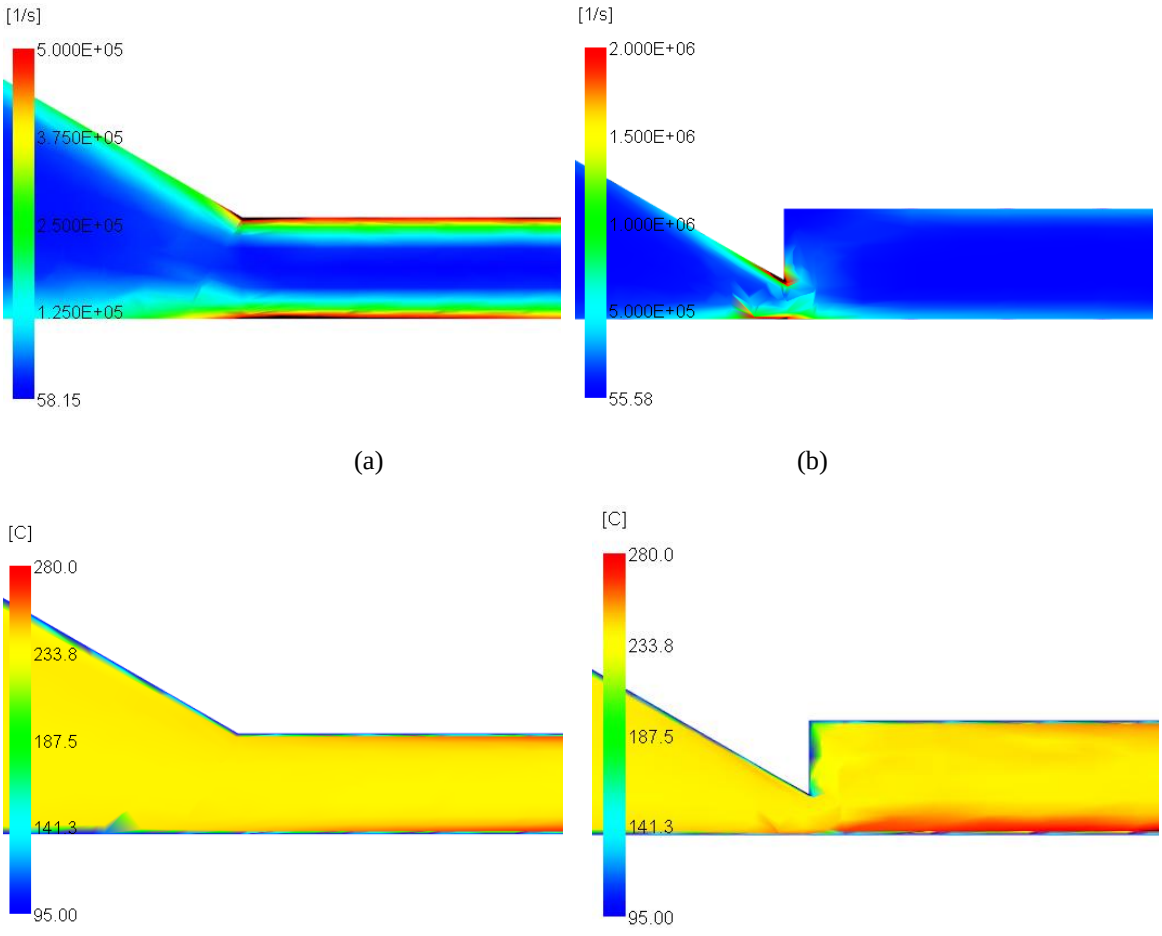

Figure 14. Distribution of the maximum shear rate of (a) gate A, (b) gate C. Temperature distribution at (c) gate A and (d) gate C. In all cases, cavity thickness is fixed to be 200μm.

Comparing the morphology of aged and non-aged specimens, there is no significant change in morphology structure and skin ratio, except for the 200μm part, as shown in Figure 15. The significant decrease of skin ratio of the 200μm part after aging may be because the sample was not cut at exactly the same position. Molecular orientations in parts at various thicknesses were examined by SWAXS, as demonstrated by the 2D scattering pattern in Figure 17. The Herman's orientation factor generally decreases with an increase of part thickness, following a similar pattern of the skin ratio. Herman's orientation factor is proportional to the skin ratio, i.e. the higher the Herman's orientation factor, the higher the skin ratio. The molecular orientation does not change after aging, as indicated by a similar scattering intensity. From the 1D WAXS data in Figure 18, samples after aging present the same scattering peak as those before aging. This indicates that the stable γ phase still exists in the material and natural aging at room temperature is not sufficient to induce any significant phase variation. The crystallinity of samples before and after aging was also tested using DSC, with Figure 19(b) showing the DSC thermographs and Table 3 listing the crystallinity and thermal data calculated from DSC thermographs. The overall crystallinity presents no monotonic variation when cavity thickness increases, since skin and core crystallinity exhibit the opposite variations when the sample thickness decreases, as reported in the literature [17]. After aging, the enthalpy of PA12 decreases for all the thicknesses, which means that the overall crystallinity decreases. This observation was found for Pebax with a high volume of soft segments, where the flexibility of PE polymer chains resulted in a reduction of PA crystals [32]. However, the same phenomenon probably also occurs for Pebax 7233. The relaxation of polymer molecular chains, especially for the soft segment, could decrease the crystallinity. Additionally, it is also interesting to see an exothermal peak immediately before the endothermic peak (160^{o}C) from the DSC thermographs, as shown in Figure 18 (b). This phenomenon resembles cold crystallization, where an exothermic peak occurs between the glass transition temperature and melting temperature during heating [33, 34]. The enthalpy of cold crystallization increases for all thicknesses after aging, except for the 100μm parts, where no cold crystallization peak is present; it may be, however, that the cold crystallization peak is too small in the small volume of the 100μm part to be detected by DSC. This means that the region of amorphous PA12 chains or imperfect PA12 crystals (small crystals) can continue crystallizing during aging, although this process is slow. Molecular relaxation not only decreases crystallinity, but it also provides a chance for cold crystallization to occur.

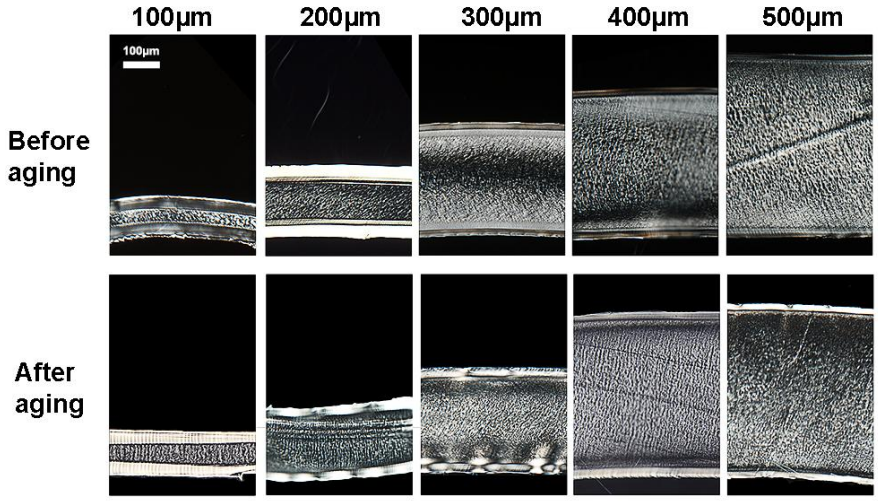

Figure 15. Morphology of part with different thickness of 22 days after moulding (before aging) and 401 days after moulding (after aging).

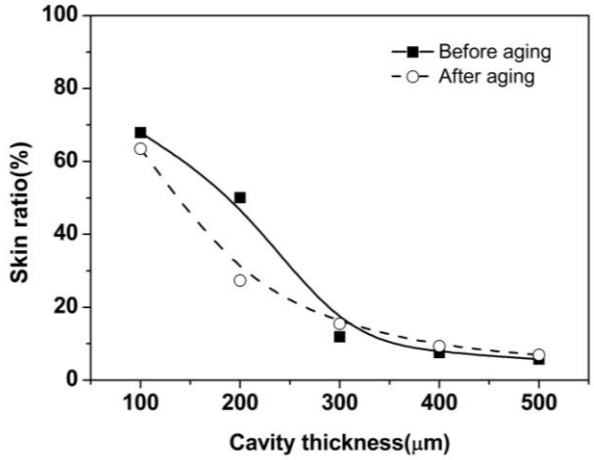

Figure 16. Skin to thickness ratios for various cavity thicknesses before and after aging.

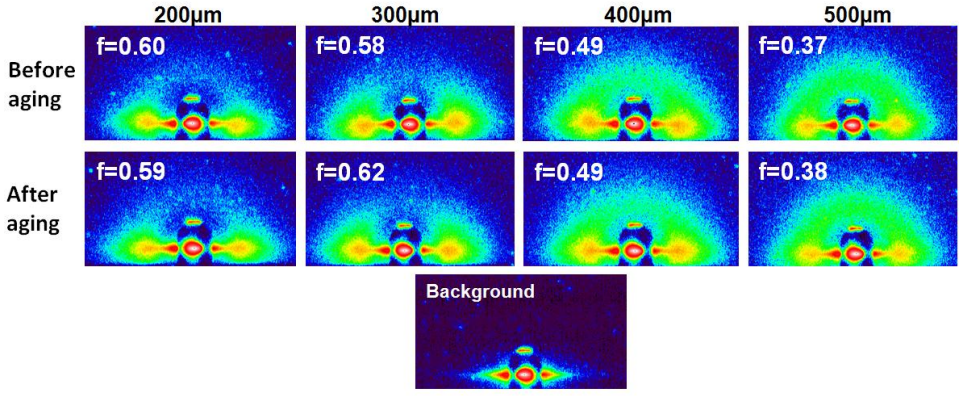

Figure 17. 2D scattering patterns from 100~500μm before and after aging.

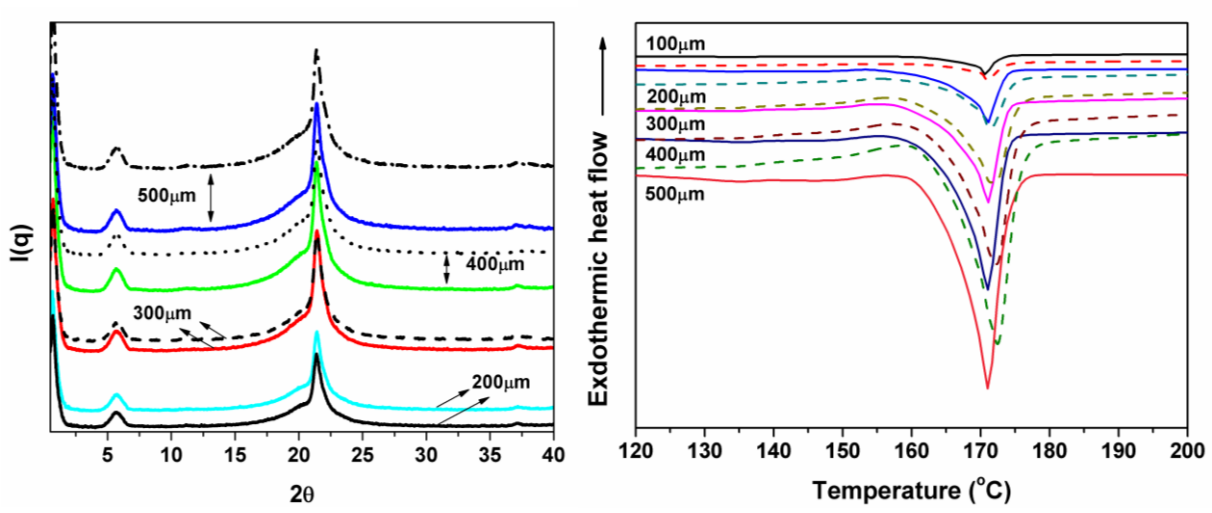

(a) (b)

Figure 18. 1D scattering patterns (a) and DSC thermograph (b) from 100~500μm thick specimens before and after aging and (solid line: before aging; dotted line: after aging).

Table 3. DSC thermal data before and after aging.

Sample thickness(μm)	T_m (°C)		ΔH_{PA12} (J/g)		ΔH_C (J/g)		Crystallinity (%)	
	before	after	before	after	before	after	before	after
100	170.76	171	-44.21	-43.09	0	0	14.38	14.01
200	171.17	171.8	-49.71	-47.75	1.85	2.49	15.58	14.72
300	171.29	172.6	-46.58	-44.59	2.49	2.89	15.96	13.56
400	171.07	172.3	-44.48	-39.22	0	0.93	14.47	12.45
500	171.52	172.9	-45.81	-42.73	2.11	2.63	14.26	13.04

3.4 Mechanical properties

Figure 19 (a) shows that the Young's modulus decreases as cavity thickness increases, most appreciably when the thickness increases from 200μm to 400μm; this follows the variation of skin ratio and orientation factor. Such behavior was also reported for conventional injection molded parts using various thermoplastic materials (ABS, PC, POM and PP), where part thickness is more than 1mm [35]. Strain at break first increases and then decreases when cavity thickness increases from 200μm to 400μm, as shown in Figure 19 (a). The effect of process conditions suggests that elongation is related to skin ratio and molecular orientation, but it seems that a critical dimension exists beyond which structural changes play a more important role than either skin ratio or molecular orientation. This observation has also been found elsewhere [17]. Additionally, the fine-grained layer disappears when cavity

thickness is less than 200μm and the corresponding skin thickness is more than half of the cross-sectional area. Since the skin layer is composed of a fast solidification layer and oriented structures, its crystallinity is lower than in the core region where a sufficiently high temperature and cooling time allow crystallization to occur. When cavity thickness is more than 300μm, the skin area reduces to less than 20% of the entire cross-section, similar to cases where process induced crystallization was studied [21]. Yield stress broadly reduces with an increase of cavity thickness, since the skin ratio decreases, as shown in Figure 19 (b). The yield stress increases with skin ratio and molecular orientation, which is also confirmed by the effect of processing when part thickness is fixed at 400μm. The high yield stress of the skin layer is considered to be due to shish structures because fibrous crystals have high strength and a deeply penetrated texture [36]. Although shish structures are not detected by SAXS, they still exist and would enhance the yield stress. Oriented lamellae of the skin can also resist stress in the tension direction and can contribute to a higher yield stress. However, compared to standard tensile specimens (from material supplier's data), Young's modulus is approximately ~30% to 50% less, strain at break reduces by ~50%-60%, while yield stress increases by ~ 30%-65%. Our previous study on the effect of processing on mechanical properties for 400μm Pebax 7233 indicated that the Young's modulus is approximately half that of a standard tensile specimen, strain at break is 30% less than expected from material supplier data sheets, and yield stress is 1.6–2 times higher than standard samples [21]. Such comparison suggests that process induced crystallization and size induced crystallization have a similar level of influence on mechanical properties for microinjection moldings.

Aging has a certain influence on all of the studied mechanical properties, where modulus and yield stress increase by ~6%-20% and ~0-27%, respectively, while strain at break decreases by ~2%-11%. Mechanical properties of thinner samples are more susceptible to the aging effect, observed as significant differences in mechanical properties in the sequence of 200 > 300 > 400=500μm in 2-sample t-tests. Considering the morphological structures, no significant variation of skin ratio, molecular orientation and crystal structure has been detected after aging. The decrease of crystallinity and increase of cold crystallization may be responsible for the change of mechanical properties. However, this still lacks conclusive evidence and it is not yet possible to correlate them together and a full characterization and understanding of cold crystallization during natural aging would be required to confirm this. In addition, structural inhomogeneity and microstructural evolution during mechanical testing, such as in-situ observations of the deformation of oriented structures and spherulite cores and their

coordinated motion during stretching, are also important in understanding the role of morphology features created by processing during tensile deformation [37].

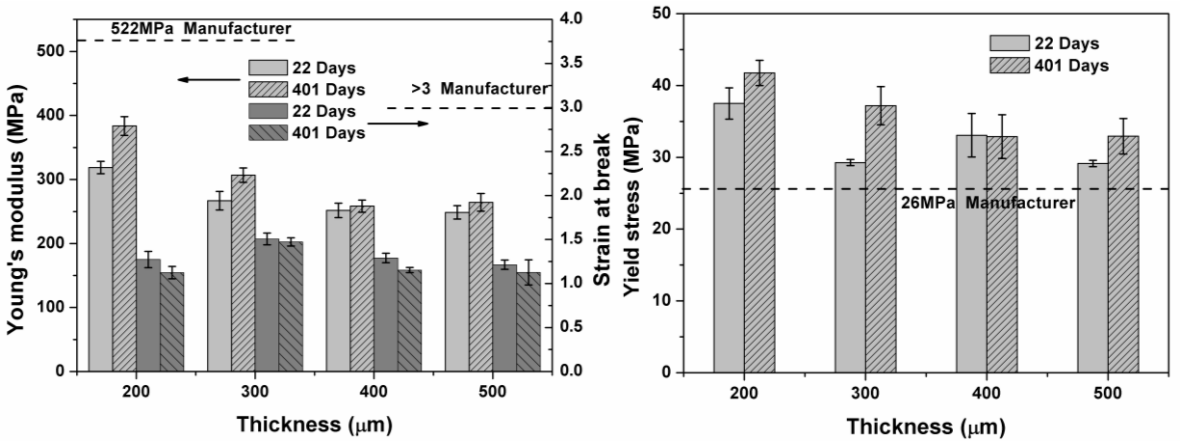

(a) (b)

Figure 19. Effect of cavity thickness on mechanical properties: (a) Young's modulus and strain at break, (b) Yield stress.

4. Conclusion

The present work has investigated the influence of gate design and part thickness on filling, morphology and mechanical properties of miniaturized dumbbell specimens. From the perspective of morphology distribution, the skin thickness of a 400μm thick part reduces from the gate end to the part's end, while the thickness of the transcrystalline layer (fine grained and oblate) generally increases, which is similar to in conventional injection molding, except for the relatively high percentage skin thickness. Some special mixtures of non-crystalline structures with a spherulite core and morphology transitions around the gate are related to shear heating, skin re-melting and flow field distribution. 100μm features also present this "skin-core" morphology and contain only a fast solidification layer and spherulite core layer, and the spherulites disappears when the feature size decreases to 20μm. A special skin bending is found to occur around 100μm size features close to the gate, because of the high melt pressure in the holding stage.

The effect of a gate on filling exhibits a complex behavior: on the one hand, the reduced thickness introduces additional heat by shear heating and helps filling; on the other hand, it increases the surface to volume ratio, and thus the cooling rate, thereby reducing filling. The gate opening in the current design has no significant effect on part

filling. Compared to the gate, an increase of part thickness can profoundly increase filling. From the morphology distribution, except for at the gate and the beginning of the part, the morphology distribution is similar with different gates. A micro gate should be designed to be thinner than the cavity thickness in order to prevent possible back flow and re-heating of the polymer melts, similar to in a conventional mold design. However, determination of an optimized gate size requires numerical modeling at the micro scale.

Mechanical analysis plays an important role in product design, which provides information about stress and strain when material properties and boundary conditions are given. Measurement of mechanical properties relies on material, processing conditions, geometry and testing methods. Important mechanical properties measured from standard tensile specimens (typically 4mm thick) as stored in a material supplier's database or a mould flow modeling database cannot represent the actual product characteristics when manufactured using particular processing conditions and small thicknesses. At best, they can only serve to provide a general and qualitative comparison. The present work and previously published literature are consistent on agreeing the following characteristics for micro injection moldings: (i) geometry scale-down to the micro scale involves high shear rates and high thermal gradients, which modify the morphology of a final product and makes it sensitive to processing conditions; (ii) size induced crystallization and process induced crystallization both create a high volume of oriented structures (surface layer); (iii) such an increase of the volume of oriented structures are primary factors to influence the short-term and long term behavior, leading to higher modulus, higher strength and lower elongation, although these properties have considerable difference from their designated values when measured using standard tensile specimens. The quality of part design depends critically on the availability and accuracy of the required material properties. In terms of sensitivity of process and size induce crystallization for microinjection moldings, the measurement of mechanical properties at micro scale is necessary for a successful micro product design.

Acknowledgement

The authors gratefully acknowledge financial support from Enterprise Ireland (Grant Nos. CFTD/07/314, CF/2012/2022 and CF/2012/2640B) and European Regional Development Fund. The authors also wish to thank Dr. Wilhelm Risse and Dr. Robert Collins of UCD for their generous assistance in DSC work.

References

[1] Yang C, Yin X-H, Cheng G-M. Microinjection molding of microsystem components: new aspects in improving performance. Journal of Micromechanics and Microengineering. 2013;23:093001.
[2] Zhang N, Chu JS, Byrne CJ, Browne DJ, Gilchrist MD. Replication of micro/nano-scale features by micro injection molding with a bulk metallic glass mold insert. Journal of Micromechanics and Microengineering. 2012;22:065019.
[3] Zhang N, Byrne CJ, Browne DJ, Gilchrist MD. Towards nano-injection molding. Materials Today. 2012;15:216-21.
[4] Jungmeier A, Ehrenstein GW, Drummer D. New aspects of process induced properties of microinjection moulded parts. Plastics, Rubber and Composites. 2010;39:308-14.
[5] Julien G, Thierry C, Patrice M. Microinjection molding of thermoplastic polymers: morphological comparison with conventional injection molding. Journal of Micromechanics and Microengineering. 2009;19:025023.
[6] Kamal MR, Chu J-S, Derdouri S, Hrymak A. Morphology of microinjection moulded polyoxymethylene. Plastics, Rubber and Composites. 2010;39:332-41.
[7] Giboz J, Spoelstra AB, Portale G, Copponnex T, Meijer HEH, Peters GWM, et al. On the origin of the "core-free" morphology in microinjection-molded HDPE. Journal of Polymer Science Part B: Polymer Physics. 2011;49:1470-8.
[8] Janeschitz-Kriegl H, Eder G. Shear induced crystallization: a relaxation phenomenon in polymer melts: a re-collection. Journal of Macromolecular Science, Part B. 2007;46:591-601.
[9] Hiroshi I, YagisawaYusuke, Takushi S, Toshiyuki Y, Takeshi K, Yoshitoshi Y. Fundamental study on structure development of thin-wall injection molded products. Theoretical and Applied Mechanics Japan 2005;54:263-8.
[10] Zhang N, Gilchrist MD. Characterization of microinjection molding process for milligram polymer microparts. Polymer Engineering & Science. 2014;54:1458-70.
[11] Liu F, Guo C, Wu X, Qian X, Liu H, Zhang J. Morphological comparison of isotactic polypropylene parts prepared by micro-injection molding and conventional injection molding. Polymers for Advanced Technologies. 2012;23:686-94.
[12] Guo C, Liu FH, Wu X, Liu H, Zhang J. Morphological evolution of HDPE parts in the microinjection molding: Comparison with conventional injection molding. Journal of Applied Polymer Science. 2012;126:452-62.
[13] Yang C. Flow-induced morphology evolution of uniformly miniaturized high-density polyethylene parts prepared by micro-injection molding. The International Journal of Advanced Manufacturing Technology. 2013;68:1745-55.
[14] Haberstroh E, Brandt M. Determination of mechanical properties of thermoplastics suitable for microsystems. Macromolecular Materials and Engineering. 2002;287:881-8.
[15] Katti SS, Schultz M. The microstructure of injection-molded semicrystalline polymers: A review. Polymer Engineering & Science. 1982;22:1001-17.
[16] Viana JC, Cunha AM, Billon N. The effect of the skin thickness and spherulite size on the mechanical properties of injection mouldings. Journal of Materials Science. 2001;36:4411-8.
[17] Meister S, Jungmeier A, Drummer D. Long-term properties of injection-molded micro-parts: influence of part dimensions and cooling conditions on aging behavior. Macromolecular Materials and Engineering. 2012;297:994-1004.
[18] Zhang K, Lu Z. Analysis of morphology and performance of PP microstructures manufactured by micro injection molding. Microsyst Technol. 2008;14:209-14.
[19] Lu Z, Zhang K. Morphology and mechanical properties of polypropylene micro-arrays by micro-injection molding. The International Journal of Advanced Manufacturing Technology. 2009;40:490-6.
[20] Lu Z, Zhang K. Crystal distribution and molecule orientation of micro injection molded polypropylene microstructured parts. Polymer Engineering & Science. 2009;49:1661-5.
[21] Zhang N, Choi SY, Gilchrist MD. Flow induced crystallization of poly (ether-block-amide) from the microinjection molding process and its effect on mechanical properties. Macromolecular Materials and Engineering. 2014;DOI: 10.1002/mame.201300459.
[22] Kantz MR. The effects of melt processing variables on the morphology and properties of injection molded polypropylene. International Journal of Polymeric Materials. 1974;3:245-58.
[23] Xie PC, Guo FX, Jiao ZW, Ding YM, Yang WM. Effect of gate size on the melt filling behavior and residual stress of injection molded parts. Mater Design. 2014;53:366-72.
[24] Pantani R, De Santis F, Brucato V, Titomanlio G. Analysis of gate freeze-off time in injection molding. Polymer Engineering & Science. 2004;44:1-17.
[25] Tor S, Loh N, Khor K, Yoshida H. The effects of gate size in powder injection molding. Material and Manufacturing Process. 1997;12:629-40.

[26] Xie L, Ziegmann G. Effect of gate dimension on micro injection molded weld line strength with polypropylene (PP) and high-density polyethylene (HDPE). The International Journal of Advanced Manufacturing Technology. 2010;48:71-81.
[27] Armstrong S, Freeman B, Hiltner A, Baer E. Gas permeability of melt-processed poly(ether block amide) copolymers and the effects of orientation. Polymer. 2012;53:1383-92.
[28] Göschel U. Two-dimensional small-angle X-ray scattering studies on oriented poly(ethylene terephthalate) films. Polymer. 1995;36:1157-65.
[29] Chu J-S, Kamal MR, Derdouri A, Hrymak A. Morphology development in the gate region of microinjection-molded thermoplastics. Polymer Engineering & Science. 2012;52:787-94.
[30] Clark ES. Morphology and properties of injection molded crystalline polymer. Applied Polymer Symposium. 1974;24:45-53.
[31] Clark ES. Structure development in injection molding acetal homopolymer. Applied Polymer Symposium. 1973;20:325-32.
[32] Todros S, Natali AN, Piga M, Giffin GA, Pace G, Di Noto V. Interplay between chemical structure and ageing on mechanical and electric relaxations in poly (ether-block-amide). Polymer Degradation and Stability. 2013;98:1126-37.
[33] Luo W-a, Liao Z, Yan J, Li Y, Chen X, Mai K, et al. Cold-crystallization of poly(trimethylene terephthalate) studied by photoluminescence of its amorphous portion. Macromolecules. 2008;41:7513-8.
[34] Mano JF, Wang Y, Viana JC, Denchev Z, Oliveira MJ. Cold crystallization of PLLA studied by simultaneous SAXS and WAXS. Macromolecular Materials and Engineering. 2004;289:910-5.
[35] Yves Vordermann FE, Johannes Kunz. Specimen thickness affects mechanical properties. Kunststoffe international. 2013;9:102-5.
[36] Fujiyama M, Wakino T, Kawasaki Y. Structure of skin layer in injection-molded polypropylene. Journal of Applied Polymer Science. 1988;35:29-49.
[37] Shinohara Y, Yamazoe K, Sakurai T, Kimata S, Maruyama T, Amemiya Y. Effect of structural inhomogeneity on mechanical behavior of injection molded polypropylene investigated with microbeam X-ray scattering. Macromolecules. 2012;45:1398-407.